Journal of
Composites Science

MDPI

Article

Influence of Multiaxial Loading and Temperature on the Fatigue Behaviour of 2D Braided Thick-Walled Composite Structures

Tim Luplow [1,*], Jonas Drummer [2], Richard Protz [3], Linus Littner [4], Eckart Kunze [3], Sebastian Heimbs [1], Bodo Fiedler [2], Maik Gude [3] and Marc Kreutzbruck [4]

[1] Institute of Aircraft Design and Lightweight Structures (IFL), Technische Universität Braunschweig, Hermann-Blenk-Str. 35, 38108 Braunschweig, Germany; s.heimbs@tu-braunschweig.de
[2] Institute of Polymers and Composites (IPC), Hamburg University of Technology, Denickestraße 15, 21073 Hamburg, Germany; jonas.drummer@tuhh.de (J.D.)
[3] Institute of Lightweight Engineering and Polymer Technology (ILK), Dresden University of Technology, Holbeinstr. 3, 01307 Dresden, Germany; richard.protz@tu-dresden.de (R.P.)
[4] Institut für Kunststofftechnik, University of Stuttgart, Pfaffenwaldring 32, 70569 Stuttgart, Germany
* Correspondence: t.luplow@tu-braunschweig.de; Tel.: +49-531-391-9933

Abstract

While size effects in composite structures have been widely studied under quasi-static uniaxial loading, their influence under fatigue conditions, particularly in the presence of multiaxial stress states and elevated temperatures, remains insufficiently understood. This study investigates the fatigue behaviour of thick-walled ±45° braided glass fibre-reinforced polyurethane composite box structures under varying temperature and loading conditions. A combined experimental approach is adopted, coupling quasi-static and fatigue tests on large-scale structures with reference data from standardised coupon specimens. The influence of temperature (23–80 °C) and multiaxial shear–compression loading is systematically evaluated. The results demonstrate a significant temperature-dependent decrease in compressive strength and fatigue life, with a linear degradation trend that aligns closely between the box structure and coupon data. Under moderate multiaxial conditions, the fatigue life of box structures is not significantly impaired compared to uniaxial test coupon specimens. Complementary non-destructive testing using air-coupled ultrasound confirms these trends, demonstrating that guided-wave phase-velocity measurements capture the evolution of anisotropic damage and are therefore suitable for in situ structural health monitoring applications. Furthermore, these findings highlight that (i) the temperature-dependent fatigue behaviour of thick-walled composites can be predicted using small-scale coupon data and (ii) small shear components have a limited impact on fatigue life within the studied loading regime.

Keywords: composites; thick-walled structures; manufacturing; braiding technology; multiaxial testing; size effect; non-destructive testing; ultrasonic testing; automation

Academic Editor: Huimin Li

Received: 5 August 2025
Revised: 22 August 2025
Accepted: 31 August 2025
Published: 4 September 2025

Citation: Luplow, T.; Drummer, J.; Protz, R.; Littner, L.; Kunze, E.; Heimbs, S.; Fiedler, B.; Gude, M.; Kreutzbruck, M. Influence of Multiaxial Loading and Temperature on the Fatigue Behaviour of 2D Braided Thick-Walled Composite Structures. *J. Compos. Sci.* **2025**, *9*, 481. https://doi.org/10.3390/jcs9090481

1. Introduction

Fibre-reinforced polymers (FRP) are widely used in various engineering fields, such as the wind energy, aerospace, and automotive industries, because of their high specific strength and stiffness. Although early applications focused primarily on secondary components, these materials are increasingly being used in critical load-bearing structures, which often require substantial wall thickness. Notable applications include aircraft landing gear attachments [1,2] and wound hydraulic bladder accumulators [3]. Another typical

application is the spar caps of wind turbine rotor blades [4], which are predominantly unidirectionally reinforced but also contain a proportion of biaxial fibres. With blade lengths exceeding 100 m, the thicknesses of spar caps can easily reach 100 mm [5], highlighting the need for robust design and manufacturing approaches to accommodate the increasing dimensions and loads of these structures.

As the range of applications expands, understanding the size-dependent behaviour of FRP has become a critical challenge to ensure reliable large-scale structural design. This challenge ranges from the complexities of manufacturing large-scale composite laminates, through the performance of mechanical tests in different loading scenarios, to the implementation of non-destructive evaluation techniques to accurately assess the progression of damage [3].

The manufacturing of thick-walled FRP laminates is more complex and requires higher quality standards than that of thin-walled composites. As thickness increases, the likelihood of manufacturing defects, such as fibre misalignment, resin-rich zones, and voids, increases, thereby affecting the local and global mechanical behaviour of the laminate [6,7]. In addition, the exothermic nature of thermoset resins makes uniform curing difficult; thick sections retain heat, leading to local overheating, resin degradation, and residual stresses that can trigger delamination [8–10]. Different manufacturing methods (e.g., liquid infusion processes, prepreg-based approaches, and pultrusion) must therefore be carefully adapted to mitigate these thermal and flow problems. Techniques such as multi-stage cure cycles and numerical process optimisation help control the temperature profile and maintain consistent fibre volume [11]. In addition, process-induced fibre undulations, which are particularly prevalent in braided or filament-wound composites, can reduce mechanical performance by creating stress concentrations [12]. Furthermore, quality assurance is more challenging with thicker laminates and non-destructive evaluation methods (e.g., ultrasound or X-ray scanning) require tailored approaches to detect subsurface defects. Together, these factors emphasise the importance of understanding how manufacturing parameters directly influence the structural integrity and design reliability of thick-walled FRP.

Despite careful process adjustments to mitigate thermal gradients and manufacturing defects, the true performance of thick-walled FRP can only be verified by rigorous mechanical testing. A central concept in this context is the so-called size effect, which suggests that mechanical properties, particularly strength, may decrease with increasing specimen thickness or overall dimensions [13]. Originally studied in brittle materials, size effect research on FRP gained momentum in the 1990s as these materials were adopted for larger, load-bearing applications. Two main theories, statistical (e.g., Weibull-based [14]) and fracture-mechanical (e.g., Bažant's law [15]), provide frameworks for explaining thickness-dependent failure behaviour. However, a variety of additional factors can aggravate these effects, including manufacturing quality, test boundary conditions, free-edge effects, stress gradients under bending, and self-heating under cyclic loading. Although many studies have investigated the quasi-static size effect in FRPs [16–19], a smaller number address these phenomena under fatigue loading [20,21].

Since early-stage fatigue damage occurs at the microscopic level, volumetric non-destructive testing (NDT) methods such as X-ray radiography may not be sensitive enough to detect such subtle changes. In contrast, ultrasonic techniques—particularly the evaluation of phase velocity in guided waves—often appear more suitable, as they are sensitive to changes in material stiffness and can detect early degradation processes before macroscopic defects become apparent [22]. Furthermore, polarised shear waves are applicable as their phase velocity is significantly affected by the shear modulus [23], which deteriorates under multiaxial loading conditions [24].

Recent studies have begun to examine the fatigue behaviour of thick-walled FRP under multiaxial loading conditions. This is particularly relevant for components that are exposed to combined stress states during service life. In [25], a biaxial testing approach is developed to capture interlaminar shear properties under multiaxial stress, a configuration representative of many thick-walled applications such as wound pressure vessels or structural joints. In [26], a comprehensive review of in-plane testing techniques for thick composite laminates is provided, highlighting the challenges of stress uniformity and the need for specially adapted fixtures. The foundational work in [27,28] addressed multiaxial fatigue testing in FRP, establishing key principles to simulate realistic load conditions and fatigue degradation mechanisms. These studies demonstrated that the stress ratio and load sequence can significantly alter fatigue degradation in thick laminates, therefore providing a foundation for understanding how complex stress states affect the durability and failure modes of thick composite structures. In terms of fatigue resistance, braided fibre composites exhibit both promising advantages and notable limitations when compared to conventional unidirectional or angle-ply laminates. The interlaced architecture of braided fabrics offers inherent damage tolerance, high conformability to complex geometries, and resistance to common fatigue failure modes such as delamination and matrix cracking during early fatigue life stages. Studies have shown that braided composites can endure up to 40–50% of their ultimate tensile strength over one million cycles, with failure typically occurring after limited prior visible damage, which is different from the progressive failure seen in unidirectional and woven laminates, where matrix cracking and delamination are often precursors to final failure [29]. Furthermore, braided composites tend to maintain better integrity at elevated temperatures due to reduced propagation of matrix-driven damage [30]. However, they often exhibit lower in-plane stiffness and strength, particularly in the braid direction, due to fibre undulation and non-ideal orientation, resulting in a strength reduction compared to equivalent conventional laminates [31]. Moreover, their fatigue behaviour is highly sensitive to braid angle and local fibre misalignment, necessitating precise manufacturing control [29,32].

In addition to multiaxial loading, environmental temperature significantly affects the mechanical performance of thick-walled FRP structures. General reviews have emphasised that even moderate thermal exposure can alter matrix properties and fibre–matrix interactions, potentially leading to inhomogeneous stress distributions in thick laminates [33]. Elevated temperatures have also been shown to accelerate fatigue damage and reduce residual strength under cyclic load [34]. The compressive strength and stiffness of thick-walled epoxy compounds was shown to decrease considerably with increasing temperature, primarily due to matrix softening and interlaminar delamination. Further investigations have highlighted that elevated temperatures, in combination with fibre misalignment or other manufacturing-induced defects, result in local stress concentrations that significantly reduce the compressive performance of fibre composites [35]. These findings underscore the critical role of thermal effects in mechanical design and in the evaluation of tolerance to damage of thick-walled FRP components.

However, most existing studies investigate the effects of multiaxial loading or environmental temperature in isolation, and these investigations are predominantly limited to thin-walled specimens or small-scale coupon tests. However, such simplified conditions may not capture the true complexity faced by large-scale and thick-walled FRP structures under realistic service loads. Almost none of these works considers the combined and distinct influences of multiaxial stresses and varying temperatures, despite their practical relevance for load-bearing or large-scale structures. A comprehensive understanding of these effects is essential to reliably predict and ensure the long-term structural integrity of thick-walled FRPs in demanding environments [36]. This study aims to improve the

understanding of the fatigue and damage behaviour of thick-walled FRP structures under multiaxial loading and elevated temperatures. To this end, the following specific objectives will be pursued:

- Assess the mechanical response of large-scale structures under complex loading conditions, focussing on the combined effects of multiaxial loading and temperature.
- Apply non-destructive testing methods (i.e., air-coupled ultrasound, computed tomography) to monitor internal damage evolution, providing insights for both manufacturing optimisation and fatigue behaviour.

To address these objectives, a reproducible manufacturing process was established for thick-walled FRP components, with particular attention to fibre architecture and the influence of key processing parameters on manufacturing quality. Generic thick-walled composite structures were then manufactured and subjected to multiaxial and uniaxial compressive fatigue tests at various temperatures. This experimental framework enables a systematic and independent investigation of the effects of multiaxiality and temperature on fatigue performance.

2. Materials and Methods

Based on preliminary design analysis, a thick-walled composite box structure was selected (Figure 1) to meet the specified requirements, such as a minimum wall thickness of 10 mm, while providing realistic geometric complexity. In particular, this configuration accommodates multiaxial loading scenarios, allowing combined compression, shear, and torsional tests, within the force capacity of the available large-scale testing facilities. In addition, this geometry can be manufactured using the intended braiding process (see Section 2.1) and, when tested under vertical and/or horizontal loads, produces relatively uniform shear forces in the webs and normal force flows in the other regions. In addition, the box design includes planar areas for coupon extraction and ensures accessibility for non-destructive testing, providing a practical compromise between structural requirements and controlled manufacturing parameters.

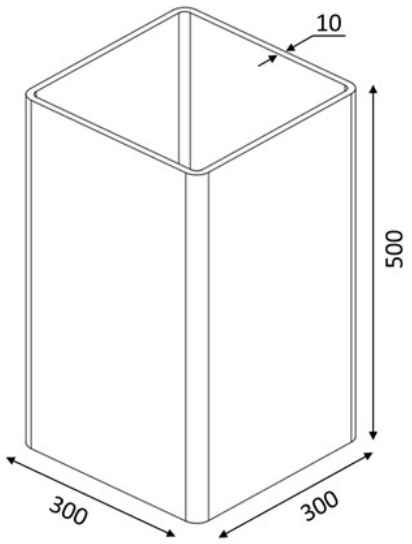

Figure 1. Schematic depiction and dimensions of the box structures in millimetres.

By systematically investigating each step of the process, from manufacturing to mechanical evaluation, the comprehensive knowledge required to reliably evaluate thick-walled braided FRP components is gained.

2.1. Manufacturing of Box Structures

The box-shaped test structures are manufactured using the direct braiding preforming process, followed by infiltration using the high-pressure resin transfer moulding (RTM) process. SE 1200 Type 30® glass (Owens Corning, Toledo, OH, USA) fibre roving was selected as the fibre material. This single-end roving has a tex value of 2400 and comprises approximately 4500 filaments, each with a diameter of 16 µm. These glass fibres are used to produce braided preforms with a 2 × 2 twill weave and a braiding angle of ±45°, using a RF 1/288-100 (Herzog GmbH, Oldenburg, Germany) radial braiding machine (Figure 2). The braiding core is automatically moved through the braiding eye of the braiding wheel by a Kuka KR210 industrial robot. A total of 288 glass fibre-fitted bobbins are used, resulting in a theoretical coverage rate of 99.9%. The 16-layer preform structure results in a preform weight of 9043 ± 157 g.

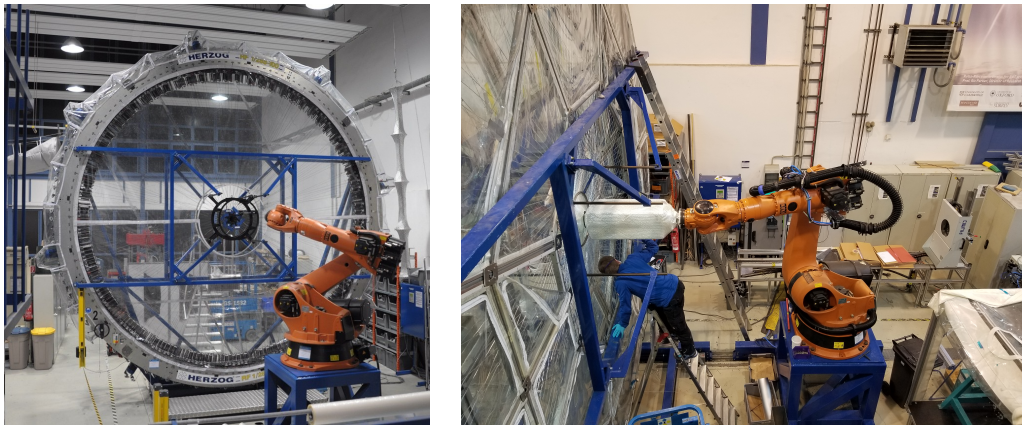

(**a**) (**b**)

Figure 2. Braiding setup used for preform manufacturing. (**a**) Radial braiding machine Herzog RF 1/288-100. (**b**) Braiding core with braided glass fibre preform.

The dry fibre preforms were infiltrated using a PUReMix high-pressure metering system (Frimo GmbH, Lotte, Germany) in combination with a shuttle-type mould carrier (KraussMaffei Technologies GmbH, Parsdorf, Germany), which provides a clamping force of 2000 kN and a clamping area of 2400 mm × 1800 mm (see Figure 3a). As matrix system, a two-component polyurethane resin (PUR) was used (Loctite Max 2, Henkel AG, Düsseldorf, Germany). The PUR offers low viscosity and fast cure at moderate temperature, allowing robust impregnation of the thick preforms and short cycle times. An internal release agent (FRP 300, Henkel AG, Düsseldorf, Germany) was added to both base components. Prior to infiltration, the mould cavity was preheated to 80 °C and evacuated to a residual pressure below 2 mbar.

The resin and hardener were automatically mixed in a weight ratio of 100:132 using the high-pressure dosing unit, with the mixing head positioned directly at the injection gate. A component pressure of 120 bar and a discharge rate of 30 g/s were applied. The average mass of the injected resin was 4454 ± 77 g, corresponding to a filling time of 149 ± 2 s. The injection gate was designed as a linear sprue along the side faces of the preform and optimised in advance using PAM-RTM mould-filling simulations. Curing was performed at 80 °C for 30 min. After demoulding (Figure 3b), the structure was post-cured in an oven at 150 °C with a heating rate of 2 °C/min and a dwell time of 1 h to minimise residual stresses. Process monitoring was carried out using two type 4001 pressure–temperature sensors (Kistler Group, Winterthur, Switzerland), positioned at the inlet and outlet of the flow path. In addition to pressure and dosing parameters, the progression of the flow front was tracked in real time using phased-array ultrasonic testing [37].

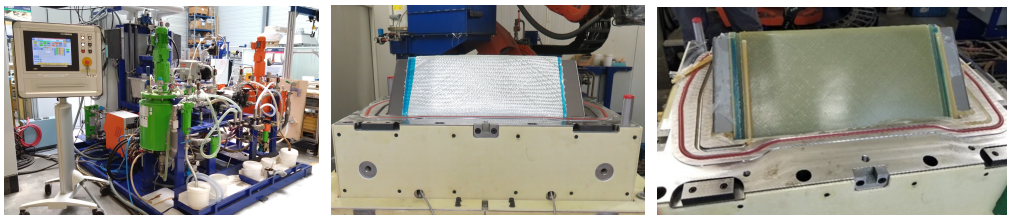

(**a**) (**b**) (**c**)

Figure 3. High-pressure RTM setup for manufacturing thick-walled composite box structures. (**a**) PUReMix high-pressure metering system for PUR resin infiltration. (**b**) Tooling with inserted preform prior to infiltration. (**c**) Mould with fully infiltrated box structure.

2.2. Destructive Testing

In order to evaluate the mechanical performance of the manufactured box structures, two different destructive testing approaches were implemented. In the first approach, the box structures were subjected to multiaxial fatigue loading on a dedicated multiaxial panel test rig, applying combined compressive and shear forces. In the second approach, uniaxial compressive tests were performed on a hexapod test rig to specifically assess the influence of environmental temperature on the fatigue behaviour. This dual testing strategy allows for a thorough investigation of the effects of multiaxial load combinations and temperature variations on the fatigue and damage mechanisms of thick-walled composite structures.

2.2.1. Multiaxial Testing

The Multiaxial Panel Test (MPT) machine has been developed at the Institute of Aircraft Design and Lightweight Structures (IFL) to evaluate large lightweight structures under combined cyclic loading (Figure 4). It consists of up to six independently controlled servohydraulic cylinders capable of applying vertical forces of up to 630 kN (cylinders 3–6) and 2 MN (cylinder 1) as well as horizontal forces of up to 1 MN (cylinder 2). The amplitude and phase of these loads are arbitrary, allowing modal and time-signal-based actuation. By arranging the cylinders vertically and horizontally, a range of load combinations can be applied simultaneously, including tension/compression and shear. The fixture accommodates structures of up to 2500 mm $\times$ 1500 mm, although smaller structures can be tested by adding stiffeners or adapters. Special guide rails maintain alignment and prevent transverse forces on the cylinders. This setup is able to apply a wide range of loading conditions, including high-amplitude cyclic loading, and allows integration of non-destructive testing for comprehensive damage assessment.

The box structure is mounted on upper and lower flat base plates that are firmly fastened to the load introduction block and heavy bolted pedestals on the bottom. The outer and inner flanges are then bolted to these plates where the box structure is introduced and embedded with a short fibre-reinforced Biresin CR120 epoxy resin (Sika AG, Baar, Switzerland) with CH120-3 hardener up to a height of 100 mm. As such, the flanges form a wedge-shaped geometry, which facilitates the absorption of vertical tensile forces. The use of short-fibre reinforcement enhances the mechanical performance of the resin by improving load transfer and crack resistance, thereby ensuring a robust clamping interface. Both the pedestal and the lower mounting fixture incorporate a centrally located opening to prevent internal pressure buildup on the structure during compressive loading. An exploded view and detailed drawings of this mounting assembly are provided in Figure 5.

As outlined in the introduction, this study investigates the multiaxial fatigue behaviour of thick-walled composite box structures subjected to cyclic compressive and shear loading. An alternating stress ratio was used to simulate realistic service conditions, in which cyclic compressive forces are combined with shear loads.

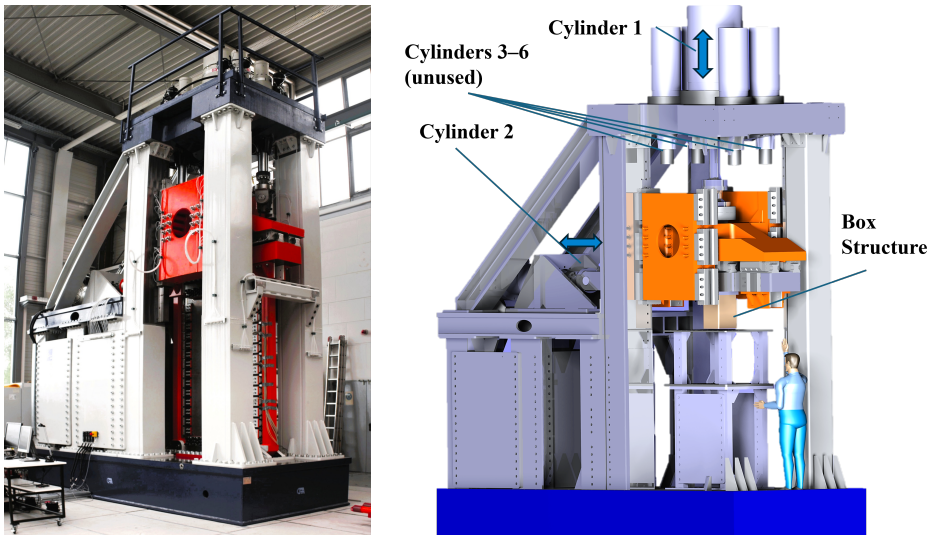

Figure 4. Multiaxial Panel Test Machine (MPT) at the Institute for Aircraft Design and Lightweight Strucures (IFL).

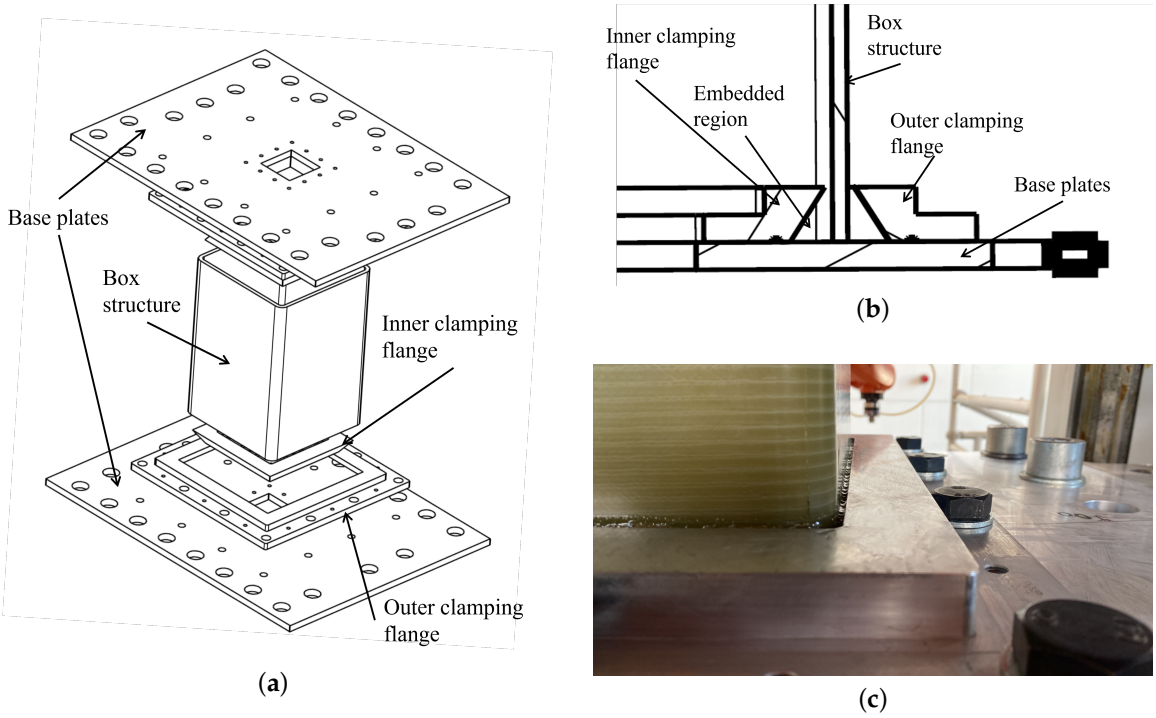

Figure 5. Fixture design for the MPT-based fatigue testing of box structures under multiaxial loading. (**a**) Exploded view of the MPT fixture setup, showing box structure and load introduction elements. (**b**) Detailed view in the area of the embedded region. (**c**) Photograph of the embedded box structure in the lower fixture.

For the experimental campaign, the MPT test rig was operated at a frequency of $f = 1$ Hz to apply cyclic compressive and shear loads, using a global stress ratio of $R = 0.1$ for both loading directions. To further investigate the effect of multiaxiality, the load ratio between axial and shear force amplitudes is introduced as

$$\alpha = \frac{F_z}{F_y} \tag{1}$$

with F_z representing the normal force and F_y the shear force, was varied during testing. Although global loading conditions were established such that the normal to shear loads

ratio corresponded to an equivalent angle of α (defined by the conventional relationship between shear stress, τ and axial stress, σ), the local stress state within individual plies does not necessarily replicate this global ratio. In practice, factors such as buckling, stiffness variations, and heterogeneous damage evolution result in significant deviations in the local stress ratio and corresponding α values in the structure. Furthermore, the horizontal load in this scenario can be applied using two distinct approaches. In the first method, a purely horizontal load is imposed while the subordinate vertical cylinder (cylinder 1) operates in a force-free manner. This leads to an induced tensile correction in the vertical direction, which results in premature failure of the embedding material and compromises the clamping of the structure. Alternatively, a controlled simple shear condition can be achieved by actively regulating the vertical cylinder to prevent any displacement in the z-direction. In this study, the second approach was selected to (1) establish a geometrically simple shear load case, although a slight overlaying compressive force in the z-direction is necessary to restrict out-of-plane movement, and (2) to prevent failure of the support matrix.

In addition to the dynamic moduli, quasi-static stiffness characterisation was performed at discrete intervals under pure compressive and shear load (e.g., at 5 kN). These periodic characterisation tests allowed for a detailed assessment of the evolution of stiffness and the progression of damage, providing valuable insights into the degradation mechanisms that govern the fatigue performance of the box structures. An exemplary load sequence and the definition of the load angle are shown in Figure 6.

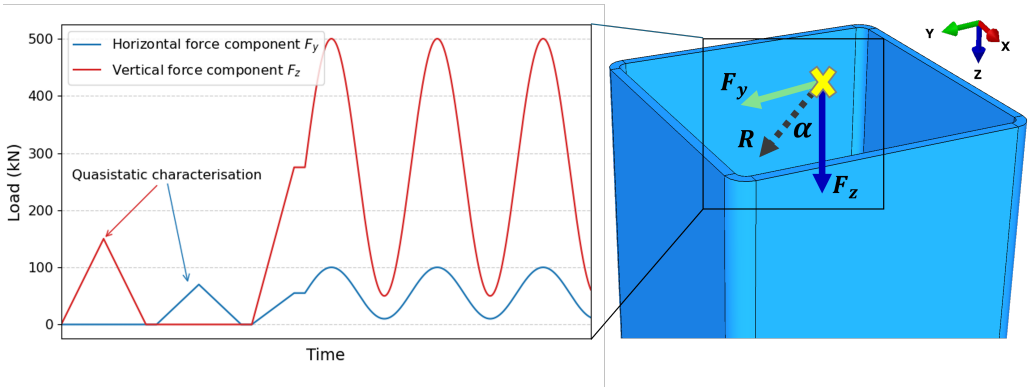

Figure 6. Schematic representation and definition of the box structure's loading sequence under multiaxial conditions.

To capture the deformation, the deformation strain gauges were applied in the vertical direction, in the horizontal direction, and in a 45° orientation in the mid-regions of the outer faces of the structure to monitor localised strain responses under multiaxial loading. One accesible shear side was reserved for the in-line NDT system, whose setup and function will be specifically described in Section 2.3.

2.2.2. Testing Under Elevated Temperatures

To investigate the temperature sensitivity of fatigue performance, additional experiments were carried out on a hexapod test platform (Figure 7a) under uniaxial loading at the Institute of Polymers and Composites (IPC). Although the MPT system enables precisely controlled multiaxial loading at room temperature, due to set-up complexity and spatial constraints, it does not support active environmental conditioning. In contrast, the hexapod setup offers full temperature control, allowing for systematic assessment of thermal effects on fatigue performance in large-scale components (Figure 7b). This approach allows a decoupled investigation of mechanical and thermal degradation mechanisms as follows: multiaxial loading was addressed under isothermal conditions using the MPT

system, whereas temperature-dependent behaviour was characterised under uniaxial loading with integrated thermal control. Combining both platforms thus enables a holistic understanding of the relevant influence factors.

The hexapod rig comprises six independently controlled hydraulic actuators, each capable of applying up to 160 kN, resulting in a total system capacity of approximately 500 kN. The ring-shaped test platform allows flexible mounting of the box structure from above, below, or within the circular frame. A closed-loop control system ensures precise positioning and load application. After each load cycle, actuation parameters are automatically adjusted to minimise deviations from the predefined displacement or force path. To enable temperature-controlled testing, a climate chamber is integrated into the test setup. As shown schematically in Figure 7c, air is heated within the chamber and introduced from above into the structure using a circulation fan. It flows downward through the box structure, is guided along the thermally insulated inner walls, and is extracted near the upper load introduction area before recirculation. The system maintains a control accuracy of ±1 °C. Surface temperature measurements at various locations confirmed a small through-thickness gradient, with the outer surface being on average 3 °C cooler than the internal cavity.

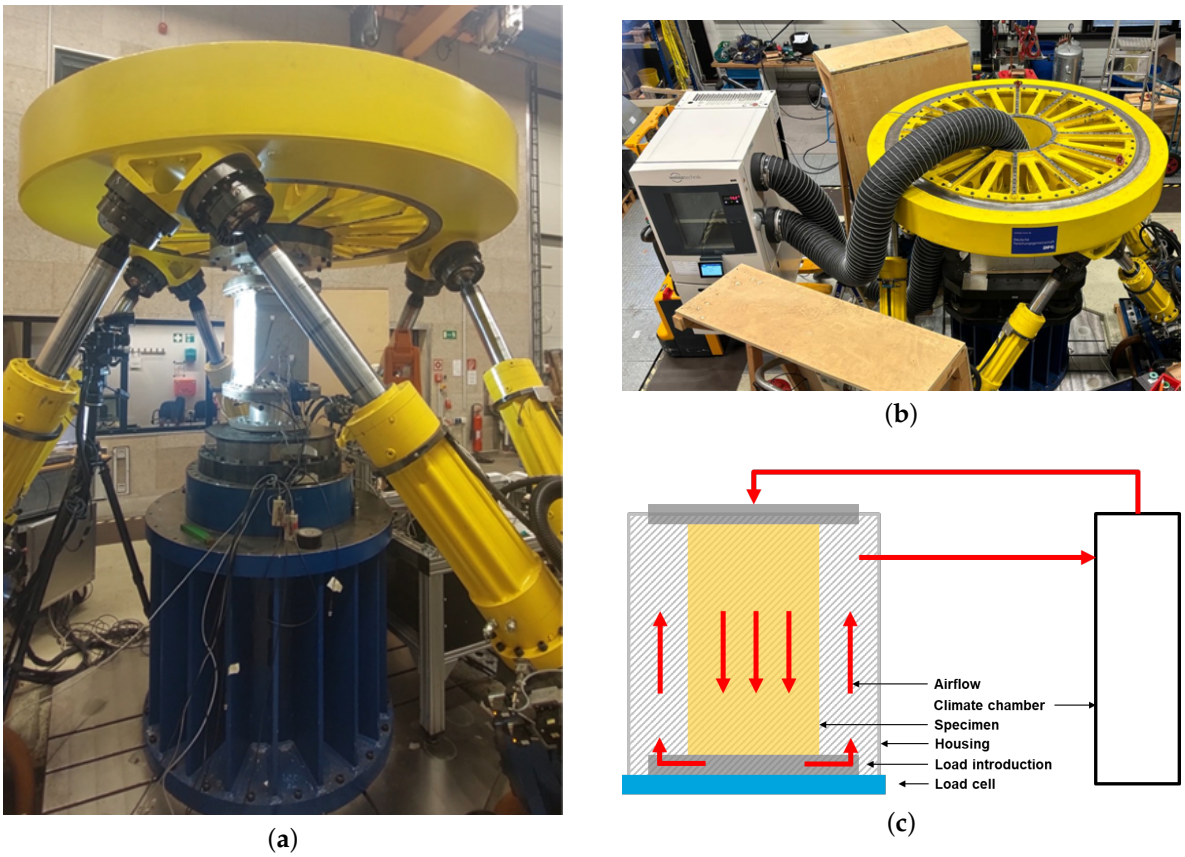

(**a**) (**b**) (**c**)

Figure 7. Hexapod-based test setup for uniaxial fatigue testing with integrated thermal control. The system enables the decoupled investigation of thermal and mechanical effects in large-scale composite structures. (**a**) Box structure mounted in the Hexapod test rig for uniaxial fatigue testing. (**b**) Box structure mounted in the circular fixture for uniaxial fatigue testing. (**c**) Schematic of the integrated climate chamber with guided airflow.

The load introduction system (Figure 8a) consists of two subsystems: a fixture system for precise positioning and embedding of the box structure and the actual force transmission unit. Before embedding, the load introduction elements (Figure 8b,c) are mounted on a base plate. The box structure is then inserted and embedded using the same material system

as in Section 2.2.1. The resin is also reinforced with short glass fibres to improve crack resistance and load transfer under multiaxial boundary conditions. Curing is performed at 70 °C for 1.5 h (3 h for the first-cast side), resulting in a glass transition temperature of approximately 100 °C. The embedded structure is then connected to the upper and lower loading units. The upper fixture is mounted on the top plate, while the lower fixture is coupled to a load cell system. Except for the lower fixture, which contains internal grooves, all elements have holes to accommodate airflow during temperature-controlled tests.

In contrast to Section 2.2.1, the tests were conducted at a frequency of 3 Hz, which is suitable due to the moderate stress amplitudes used. As the ambient temperature in the test chamber exceeded 50 °C, the effects of self-heating during cyclic loading were considered negligible. To ensure safe operation given the multiple possible degrees of freedom of the test rig, all uniaxial tests were performed in displacement control mode. Calibration measurements were used to define the required displacement amplitudes corresponding to the desired force levels. These amplitudes were periodically updated throughout the test campaign to account for material relaxation and stiffness degradation. On average, the force amplitudes remained within ±5% of their nominal values.

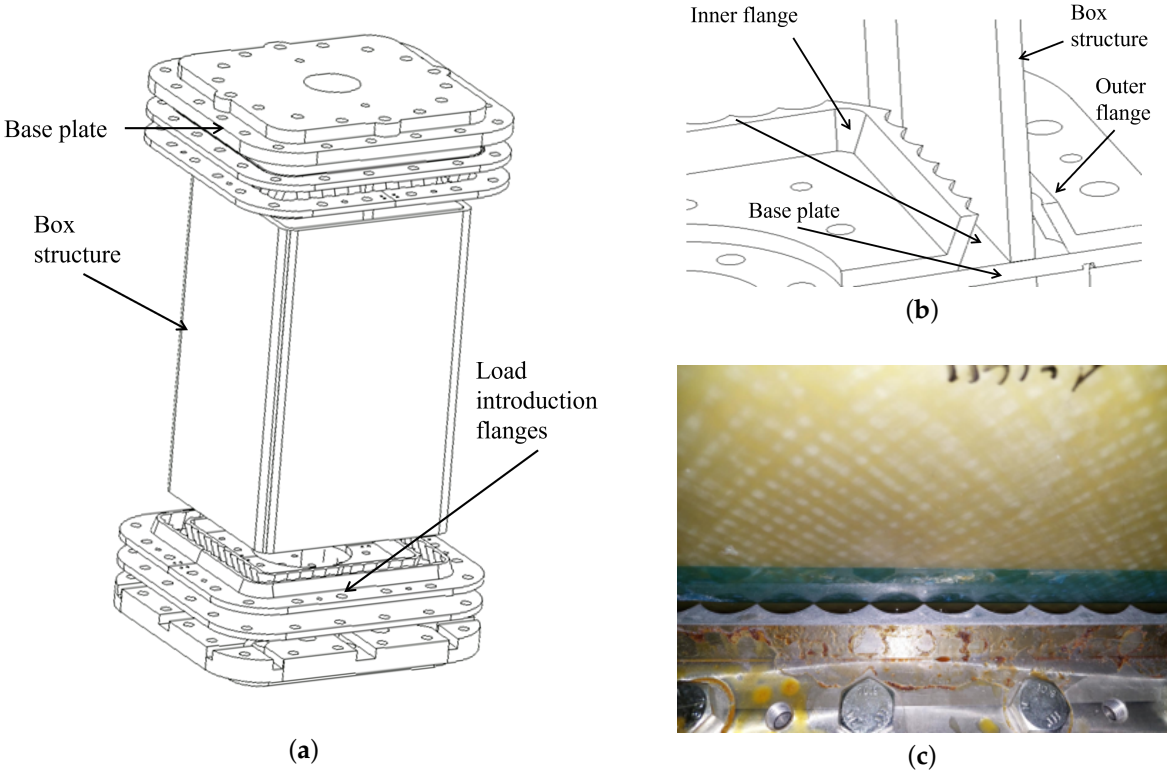

Figure 8. Fixture design for the hexapod-based fatigue testing of box structures under temperature-controlled uniaxial loading. (**a**) Exploded view of the hexapod fixture setup, showing box structure and load introduction elements. (**b**) Detailed corner view of the embedded structure. (**c**) Close-up of the lower fixture with airflow grooves.

Throughout the tests, the displacement of the hexapod platform was continuously recorded and strain monitoring was performed using two surface-mounted strain gauges. In the uniaxial setup, both gauges were aligned with the axial loading direction.

2.3. Accompanying Non-Destructive Testing

In order to effectively monitor fatigue-related damage and ensure the transferability of mechanical characterization results to future monitoring applications of FRP, a non-destructive testing system was developed. For a successful integration into the destructive

testing systems mentioned above, several key requirements must be met. Due to the geometry of the box structures and their clamping configuration, only one-sided inspection is possible. In addition, the embedding process in the load introduction block can lead to slight variations in the position of each box structure, requiring an adaptive system capable of recalibrating the inspection area for every new test structure. To ensure consistent measurements and minimise operator influence, the inspection process must also be highly repeatable and automated. Given these constraints, a robotic system was implemented to monitor degradation based on ultrasonic testing (Figure 9). The inspection system utilises an ABB IRB 120 robotic arm controlled by an IRC5 controller (both ABB Asea Brown Boveri Ltd., Zurich, Switzerland) to precisely position the ultrasonic probes during testing. The inspection area was identified at the start of the inspection procedure using a push sensor. Although measurements are prepared and initiated manually at predefined intervals, the acquisition process itself is fully automated, ensuring consistency and reducing human error. A more detailed description of the test setup can be found in [23].

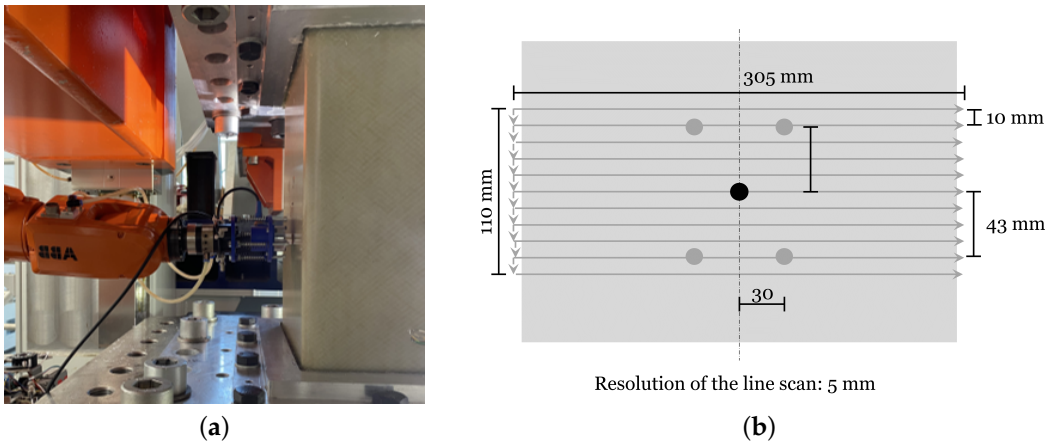

Figure 9. Automated non-destructive inspection of the composite box structure using a robotic system. (**a**) Robotic arm with the shear wave ultrasonic probe inspecting the composite box structure. (**b**) Measurement positions for shear wave (grey), Lamb wave (black), and air-coupled ultrasonic testing (arrows).

To effectively monitor fatigue-induced damage and assess changes in the material properties of the composite structures, the testing protocol encompasses three distinct procedures. One procedure involves determining the phase velocity c_{ij} of polarized shear waves. According Equation (3), the phase velocity is directly related to the material's shear modulus G_{ij},

$$c_{ij} = \sqrt{\frac{G_{ij}}{\rho}} \qquad (i,j = x,y,z) \tag{2}$$

where ρ represents the material's density. The indices i and j refer to the coordinate system of the test structure, with the 1-direction indicating the direction of the pressure load, the 2-direction in the direction of the shear load and the 3-direction in the wave propagating through thickness direction. By measuring the time of flight of the signal c_{ij}, G_{ij} can therefore be calculated (see Equation (3)), providing insights into the elastic properties of the material and enabling the detection of fatigue-related stiffness degradation.

$$c_{ij} = \frac{2d}{\Delta t_{ij}} \qquad (i,j = x,y,z) \tag{3}$$

The shear wave experiments were performed with a 1 MHz shear wave transducer (Evident Scientific Inc., Tokyo, Japan) with a 28 mm Polymethylmethacrylate (PMMA)

delay line and a SNAP RAM-5000 ultrasonic test device (Ritec Inc., Warwick, RI, USA). The transducer was exited with a 1 MHz sinus burst of two cycles and the received signal was averaged five times.

As a second test method, a precise determination of the phase velocity of Lamb waves was made at the centre of the surface of the tested box structure by varying the distance between two probes and analysing the resulting flight differences time (see Figure 10). In order to prevent a deformation-related change in the distance between the sensors, the measurement was carried out using air-coupled ultrasound. The non-contact test sequence ensures an unchanged measuring position throughout the tests. The measurements were conducted at the centre of the test box structure's surface. To systematically capture variations in phase velocity, the probe separation distance Δs was adjusted in discrete steps. To account for directional dependencies in wave propagation, each measurement was performed twice as follows: once with the wave propagation direction orthogonal to the applied compressive load (z-direction) and once parallel to it (y-direction). By analysing the resulting time-of-flight differences, the phase velocity of Lamb waves was extracted, providing further insights into the mechanical behaviour and degradation of the composite structure.

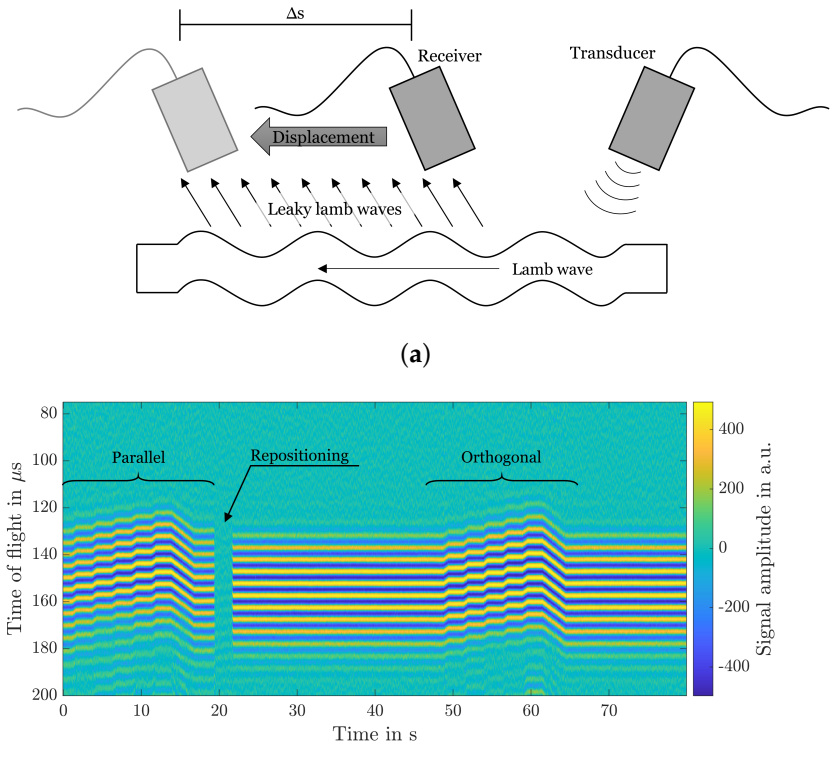

Figure 10. Air-coupled ultrasonic measurement setup and evaluation of Lamb wave phase velocity. (**a**) Schematic measurement setup of the air-coupled ultrasonic measurement. (**b**) Results of the transit time measurement to determine the phase velocity of the Lamb wave.

Lastly, an air-coupled ultrasonic test (UT) was performed on an area of 305 mm × 120 mm with a measurement grid of 5 mm × 10 mm, capturing time of flight and amplitude deviations. The test setup is a re-emission arrangement, similar to Figure 10, without the lateral movement of the receiver. Both air-coupled inspection methods were conducted using two 200 kHz air-coupled transducers (Ultran Group, State College, PA, USA), excited by a seven-cycle, 200 kHz rectangular burst. The received signals were amplified with a 46 dB low noise amplifier (Inoson GmbH, St. Ingbert, Germany), recorded with an

UltraSCOPE AIR ultrasonic testing device (Dasel SL, Madrid, Spain) and averaged 16 times. The positions of all three measurements that were performed can be derived from Figure 9b: The five dots mark the polarised shear wave points, whereas the central black dot, located at the middle of the structure's face, marks the Lamb-wave velocity measurements location. The grey arrows indicate the air-coupled UT scan path.

2.4. Reference Coupon Testing

In addition to large-scale structures, flat plates were manufactured using high pressure RTM (HD-RTM) using a biaxial braided fabric that, although not identical to the box structure preform, used the same rovings and resin system. The processing conditions were chosen to achieve the target fibre–volume fraction calculated for the box components. From each base plate, $\pm 45^\circ$ compression coupon specimens were cut according to the dimensions specified in DIN EN ISO 14126 [38].

Quasi-static compression tests at the coupon level were performed using a Z400 Zwick universal test machine at a testing speed of 1 mm/min. To avoid slippage, the machine is equipped with hydraulic grips, which grip the specimen tab with a pressure of 250 bar. The environmental temperature is regulated with a climate chamber TempEvent T/180/70a/3 (Weiss Technik, Reiskirchen, Germany) the temperature is measured directly on the coupon specimens, and it is considered permissible if the desired temperature is reached with a tolerance range of 1 °C for at least 5 min. The tests were carried out in 23 °C, 40 °C, 60 °C, and 80 °C.

The fatigue compression tests were performed on a Schenck PSB servohydraulic axial testing system at three load levels (LL1–LL3) and a fixed frequency of 1 Hz. The low test frequency was selected to limit viscoelastic self-heating of the $\pm 45^\circ$ specimens. The surface temperature was continuously monitored with thermography and, in steady state, never exceeded $\Delta T = 5\text{K}$.

3. Results and Discussion

This section summarises the experimental results of the study. First, coupon-scale investigations are presented under quasi-static and fatigue loading to establish a temperature-dependent and uniaxial reference behaviour. The discussion then moves to the thick-walled $\pm 45^\circ$ braided box structures, examining their quasi-static response and fatigue performance in detail.

3.1. Coupon Tests: Quasi-Static Strength and Fatigue Reference

Figure 11a summarises the compressive strength of the coupon specimens as a function of environmental temperature. The data reveal an almost linear degradation: the average strength decreases from $\approx$ 154 MPa at 23 °C to $\approx$ 66 MPa at 80 °C. A linear regression yields

$$\sigma_c(T)\ [\text{MPa}] \;=\; -1.49\,T\ [^\circ\text{C}] + 188.0, \tag{4}$$

with a coefficient of determination $R^2 = 0.97$. Equation (4) is used to normalise the fatigue load levels of the box structures to the quasi-static temperature-dependent capacity.

Figure 11b presents the S-N curve (Wöhler) obtained from the coupon series at 23 °C. The fatigue life exhibits the expected logarithmic decline with an increase in the stress ratio, asymptotically approaching a finite endurance limit of approximately $0.18\,\sigma_c(23\ ^\circ\text{C})$ at $N = 10^7$ cycles. No abnormal features such as multiple knee points or runout scatter are detected. These data serve as a reference for assessing the performance of the scaled box structures.

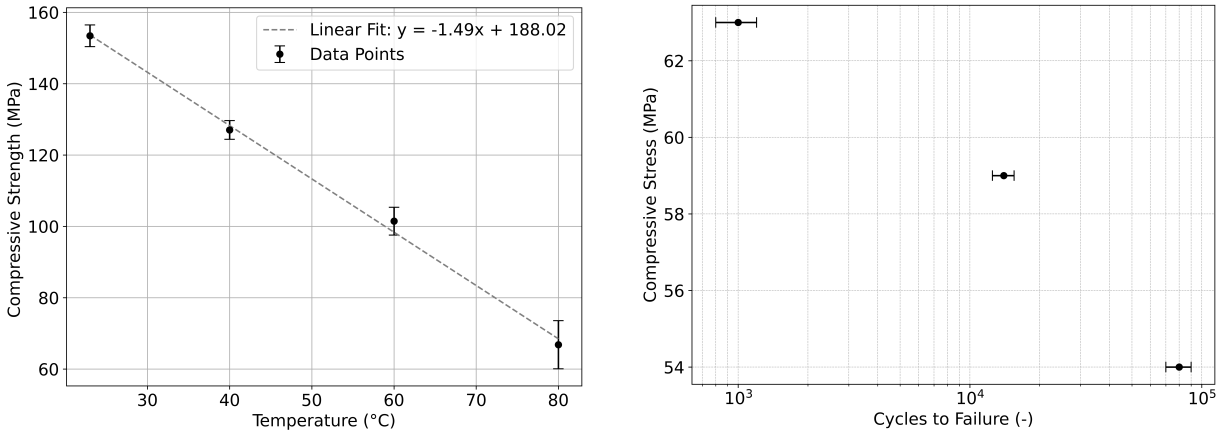

Figure 11. Coupon reference data: (**a**) Linear loss of compressive strength with temperature. Quasi-static compressive strength versus temperature. (**b**) Fatigue performance at 23 °C. Room-temperature S–N curve.

3.2. Box Structures

Table 1 provides an overview of all tested box structures (BS), including two quasi-static reference structures (BS_01, BS_02) for benchmarking. The table also highlights structures that represent run-outs, showing no global failure within the test duration. The structural tests were designed to investigate the influence of combined multiaxial loading and environmental temperature on fatigue life while maintaining a consistent geometric configuration in all samples.

Table 1. Overview of box-structure tests and principal outcomes.

Box Structure	Temperature T (°C)	Multiaxiality F_y/F_z (-)	Cycles n (-)	Rel. Vert. Load $\frac{\sigma_{max}}{\sigma_{ult,specimen}}$ (-)	Failure
BS_01	23	0	QS, vertical	0.81	yes [1]
BS_02	23	0.2	QS, horizontal	—	yes [3]
BS_03	23	0.2	2.30×10^5	0.29	no [4]
BS_04	70	0	3.82×10^5	0.25	yes [2]
BS_05	23	0.2	4.35×10^3	0.45	yes [2]
BS_06	80	0	2.08×10^5	0.25	yes [2]
BS_07	23	0.2	2.86×10^4	0.40	yes [2]
BS_08	23	0	1.00×10^6	0.25	yes [2]
BS_09	75	0	1.38×10^6	0.25	yes [2]
BS_10 (1)	23	0.2	8.10×10^3	0.15	no
BS_10 (2)	23	0.2	2.50×10^5	0.15	no
BS_10 (3)	80	0	4.76×10^5	0.25	yes [2]

[1] Buckling; [2] Compressive failure; [3] Embedding failure; [4] Run-out (test interruption before failure).

3.2.1. Preliminary Tests

Initial experiments were conducted to characterise the structural response and boundary conditions under controlled uniaxial loading. Quasi-static compression and shear tests at room temperature revealed different deformation mechanisms.

Under uniaxial compressive loading, failure was dominated by the buckling of the structure. Figure 12 shows the box structure in its unloaded state and shortly before buckling failure, illustrating the onset of localised out-of-plane deformation. The onset of buckling occurred approximately 80 % of the ultimate strength of the reference coupons,

validating the predictions of linear buckling and motivating lower load levels in subsequent fatigue tests.

Initial quasi-static tests were performed under horizontal shear loading to establish appropriate load boundaries for subsequent fatigue tests. Despite the addition of short fibres to reinforce the resin, failure consistently occurred near the load introduction zone at approximately 20 % of the maximum compressive amplitude. Based on these observations, all subsequent fatigue tests were conducted using a constant shear–compression ratio of $\alpha = 0.2$, deliberately chosen to remain below this critical threshold. Furthermore, the selected load ratio reflects realistic multiaxial loading conditions found in wind engineering applications such as turbine blades [39]. In [40], it is emphasised that representative off-axis loading is essential to capture early fatigue damage mechanisms in FRP. Thus, the chosen ratio offers a relevant basis for fatigue testing and enables a systematic assessment of the influence of moderate shear contributions on fatigue life, while reliably preventing premature failure.

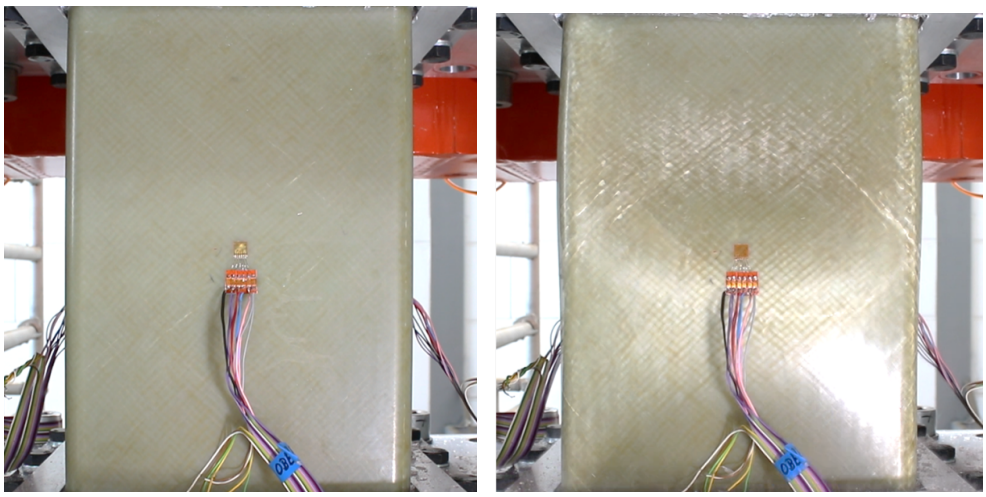

(**a**) (**b**)

Figure 12. Quasi-static compressive response of the box structure BS_01. (**a**) Unloaded state of the test structure. (**b**) Visible out-of-plane deformation preceding global buckling at 1.25 MN.

3.2.2. Influence of Multiaxial Loading

Figure 13 compares the results of the box structures tested under superimposed axial and shear loads ($F_y/F_z \approx 0.2$) with the fatigue data from the uniaxial coupon specimen. The applied multiaxiality represents a moderate deviation from pure compression. The fatigue lifetimes of the box structures fall within the scatter band of the coupon data at all three load levels (LL1–LL3), indicating that for the range investigated here, the moderate shear-compression ratio does not significantly affect fatigue performance.

To investigate local damage evolution, Figure 14 shows the progression of dynamic stiffness for the structure BS_05 throughout the cyclic loading. To evaluate stiffness degradation during fatigue, the normalised shear modulus G_n/G_0 and Young's modulus E_n/E_0 were determined from strain gauge rosette measurements in 0°, 45°, and 90° orientations, respectively. The shear strain is obtained as

$$\gamma_{xy} = 2\left(\varepsilon_{45} - \frac{\varepsilon_0 + \varepsilon_{90}}{2}\right). \tag{5}$$

Under load-controlled conditions, the applied shear stress τ_{xy} is assumed constant, allowing the normalised shear modulus to be computed from the inverse ratio of shear strains.

$$\frac{G_n}{G_0} = \frac{\gamma_0}{\gamma_n} = \frac{\varepsilon_{45}^{(0)} - \frac{\varepsilon_0^{(0)} + \varepsilon_{90}^{(0)}}{2}}{\varepsilon_{45}^{(n)} - \frac{\varepsilon_0^{(n)} + \varepsilon_{90}^{(n)}}{2}}. \tag{6}$$

Similarly, assuming loading primarily in the 0° direction, the normalised Young's Modulus is derived from the direct strain response as follows:

$$\frac{E_n}{E_0} = \frac{\varepsilon_0^{(0)}}{\varepsilon_0^{(n)}}, \tag{7}$$

assuming constant axial stress. These formulations allow a direct quantification of modulus degradation from strain data without requiring force or material parameters.

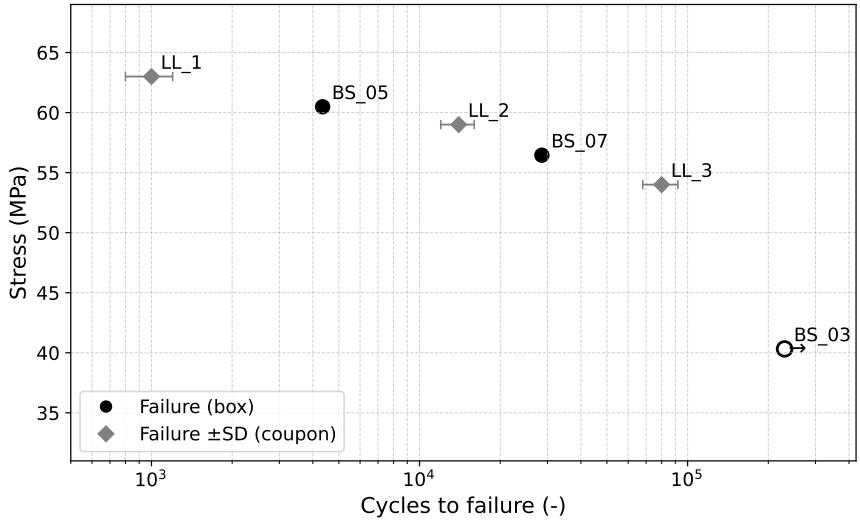

Figure 13. Comparison of box structures and coupon load levels in the S–N domain. The arrow indicates the run-out.

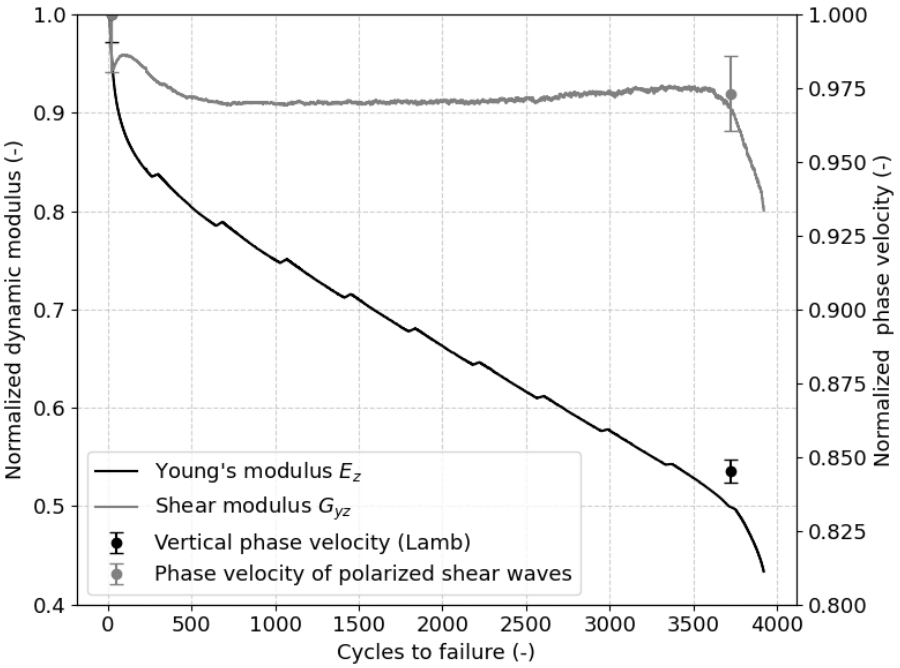

Figure 14. Dynamic stiffness degradation for structure BS_05 under multiaxial loading, complemented by NDT-based phase velocity measurements.

A pronounced decline in axial stiffness (E_z) of approximately 40% is observed prior to failure, whereas the shear stiffness (G_{yz}) remains largely stable. This discrepancy reflects the underlying fibre architecture as follows: the ±45° biaxial braid aligns the fibres with the shear direction, resulting in high stiffness and damage resistance under shear. In contrast, the axial direction is dominated by the matrix, making it more vulnerable to fatigue degradation.

Complementary non-destructive evaluation using guided wave phase velocities confirms this behaviour. The axial phase velocities (0°), which are sensitive to deviations of E_z, show a marked reduction. The reduction is not just localised at the point selected for the point measurement in the middle of the structures. The ultrasonic scans performed on the basis of Lamb waves also show a widespread increase in time of flight of the lamb waves to up to 5.6 ± 0.24 µs (see Figure 15) and thus the phase velocity. In addition, the shear wave velocity associated with the shear modulus remains nearly constant, as shown in Figure 14. The anisotropic phase velocity degradation observed in ultrasound measurements is primarily attributed to matrix cracking and interfacial debonding, which alter the effective stiffness in fibre-parallel and perpendicular directions. Although the method does not directly resolve individual damage types, the directional dependence of the wave velocity provides information on the accumulation of preferential damage aligned with the orientation of the fibre. The good agreement between stiffness loss and phase velocity degradation highlights the suitability of NDT methods for capturing anisotropic damage in fibre-reinforced composites.

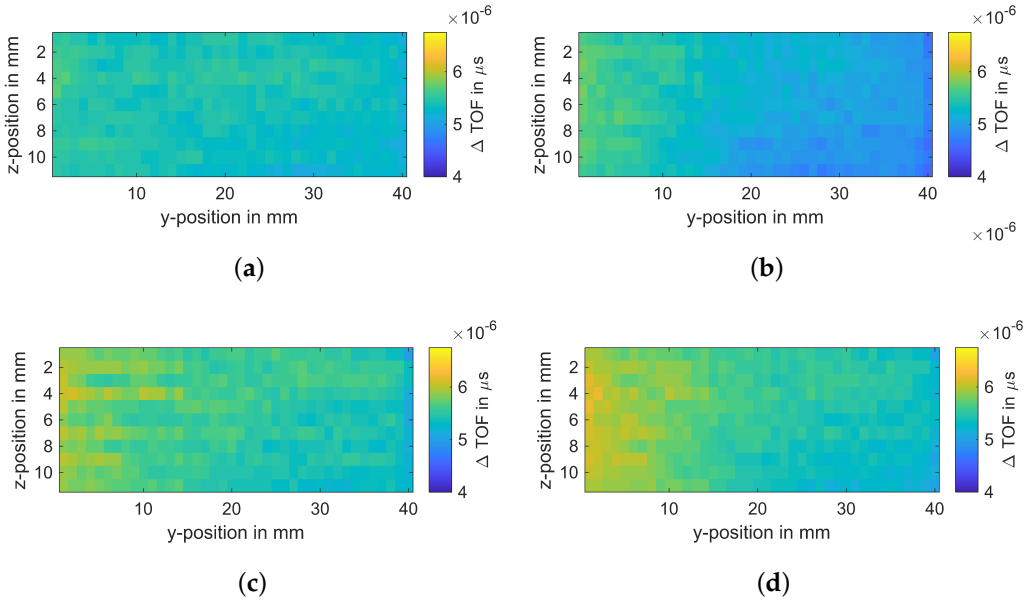

Figure 15. Difference in time of flight of the ultrasonic Lamb wave signal for box structure BS_03 under multiaxial loading for different load cycles. (**a**) 10,000 cycles. (**b**) 30,000 cycles. (**c**) 180,000 cycles. (**d**) 230,000 cycles.

These findings underscore that damage accumulation in the ±45° braided box structures is highly directional, with degradation occurring predominantly along matrix-dominated directions under the vertical loading. In contrast, the reduction in global shear stiffness remains comparatively minor. This is attributed to the inherent fibre orientation of the ±45° architecture, which is well suited to resist in-plane shear loading. Furthermore, the applied load ratio in the multiaxial tests was relatively small, resulting in limited shear-driven degradation. Although a minor shear component does not appear to significantly reduce fatigue life, it may still contribute to localised effects near geometric or material

discontinuities. The consistent results obtained from both mechanical and non-destructive monitoring confirm that wave-based techniques are capable of tracking internal damage evolution, supporting their applicability for future structural health monitoring (SHM) in service environments.

3.2.3. Influence of Elevated Temperatures

Figure 16 compares the quasi-static compressive strength of ±45° coupon specimens with the fatigue life of full-scale box structures as a function of temperature. The black markers indicate the mean strength of the coupon specimens, including standard deviation, while the red squares represent the maximum number of load cycles endured by each box structure at the respective test temperature.

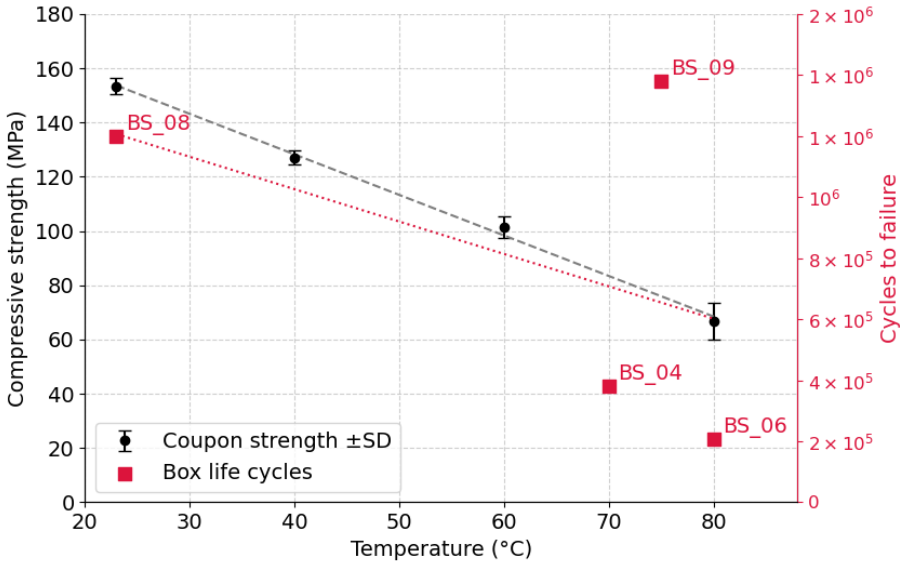

Figure 16. Comparison of temperature-dependent coupon strength (black) and box structure fatigue life (red).

A temperature-dependent reduction in fatigue resistance is evident for the box structures, and this trend closely mirrors the strength degradation observed in the coupon tests. In particular for BS_04 and BS_06, tested at 70 °C and 80 °C, a distinct drop in fatigue life corresponds with the pronounced decrease in quasi-static reference strength. This alignment supports the assumption that the coupon specimens provide a reasonable approximation of local strength reduction in the webs of the box structures.

An exception is observed for BS_09, tested at 75 °C, which achieved an unexpectedly high fatigue life compared to the coupon-based reference. Possible explanations include local differences in material quality, process-related variability, or test-specific boundary conditions. However, further specimens are required to substantiate this outlier and quantify underlying causes.

It should be noted that, due to resource limitations, only a single box structure was tested per temperature level. For completeness, the box structure BS_10 is included in the test matrix; however, it is not considered in Figure 16 due to its non-uniform load history. This specimen was tested on the hexapod test rig under varying load ratios, including torsional components and temperature variations, and primarily served as a setup validation trial. However, its observed failure response falls within the expected range and supports the general temperature-dependent fatigue trend. Consequently, the current data set allows only a qualitative evaluation of temperature-dependent effects. Statistical significance and data scatter cannot be robustly assessed at this stage. Nonetheless, the

close correspondence in trend between coupon-based quasi-static strength and structural fatigue performance strengthens the confidence in the observed degradation behaviour.

4. Conclusions

This study investigated the fatigue behaviour of thick-walled $\pm 45^\circ$ composite box structures under varying temperature and loading conditions. A combined experimental approach was used, integrating coupon-scale reference data with full-scale structural testing, to assess temperature sensitivity and the role of moderate multiaxial stress states in structural durability.

At elevated temperatures, the box structures exhibited a reduction in compressive strength and fatigue life, consistent with the linear degradation trend observed in the coupon specimens. Despite the limited number of tests per temperature, the similarity in degradation slopes suggests that coupon-scale data provide a suitable baseline for predicting structural behaviour. However, the markedly longer fatigue life of BS_09 at 75 °C, underscores the need for larger sample sizes to account for material or process variability.

With respect to multiaxial loading, box structures subjected to moderate compressive–shear interaction ($F_y/F_z = 0.2$) showed fatigue lives comparable to uniaxial coupons, indicating that such loading conditions do not significantly impair performance. Monitoring of dynamic stiffness revealed only minor shear modulus degradation, reflecting the structure's favourable fibre orientation and the relatively low shear-to-compression ratio.

In summary, the following key findings can be drawn:

- The study presents a methodology for the manufacturing and mechanical testing of thick-walled composite box structures. A combination of the braiding process, controlled HP-RTM infiltration, and multiaxial testing with integrated thermal conditioning and in situ NDT provides a transferable experimental framework for structural fatigue investigations under complex conditions.
- In compressive–shear loading, the shear-optimised box structures exhibit only minor reductions in fatigue performance and stiffness degradation at a moderate multiaxiality ratio. This indicates that the $\pm 45^\circ$ braided fibre architecture offers inherent robustness under combined compressive–shear loading.
- The temperature sensitivity of fatigue performance is well captured by small-scale coupon tests and can be extrapolated to structural scale using a linear degradation model. This correlation enables reliable life predictions of thick-walled structures based on simplified coupon testing.
- The integrated, non-destructive testing approach based on ultrasonic shear and Lamb wave velocity measurements proved effective in tracking directional stiffness degradation throughout the fatigue life of the material. Despite the complex set-up and boundary conditions, the wave-based measurements showed good agreement with the mechanical response, thus demonstrating their viability for in situ structural health monitoring.

These results form a solid basis for assessing the fatigue durability of fibre-reinforced composite structures under complex stress states and thermal exposure. However, additional tests with larger sample sizes, particularly for structural-scale samples, are required to assess the repeatability of the results, quantify statistical variability, and enhance the robustness of fatigue life predictions under varying temperature and loading conditions. To further generalise the findings, future investigations should also explore higher shear-compression ratios, where more severe shear–compression interactions may induce different failure modes or accelerate damage evolution. In addition, broadening the scope of the material to alternative fibre architectures and incorporating in situ monitoring approaches could improve the mechanistic understanding of fatigue degradation. Finally, studying

combined environmental effects such as humidity or thermal cycling would improve the transferability of these results to real-world service conditions.

Author Contributions: Conceptualization, T.L. and J.D.; Data curation, R.P.; Formal analysis, T.L., J.D. and L.L.; Funding acquisition, S.H., B.F., M.G. and M.K.; Investigation, T.L., J.D., R.P., L.L. and E.K.; Methodology, T.L., J.D., R.P., L.L. and E.K.; Project administration, S.H., B.F., M.G. and M.K.; Resources, S.H., B.F., M.G. and M.K.; Supervision, S.H., B.F., M.G. and M.K.; Validation, T.L., J.D., R.P., L.L. and E.K.; Visualization, T.L., J.D., R.P., L.L. and E.K.; Writing—original draft, T.L., J.D., R.P., L.L. and E.K.; Writing—review and editing, T.L., S.H., B.F., M.G. and M.K. All authors have read and agreed to the published version of the manuscript.

Funding: This research and was funded by the Deutsche Forschungsgemeinschaft (DFG) and is part of the PAK 988 project with the subprojects 428326921, 428328210, 428323347, and 428324840. We would like to take this opportunity to thank the DFG for the financial support.

Institutional Review Board Statement: Not applicable.

Informed Consent Statement: Not applicable.

Data Availability Statement: The data presented in this study are available upon request from the corresponding author.

Conflicts of Interest: The authors declare no conflict of interest.The funders had no role in the design of the study; in the collection, analyses, or interpretation of data; in the writing of the manuscript; or in the decision to publish the results.

Abbreviations

The following abbreviations are used in this manuscript:

CT	Computer tomography
IFL	Institute of Aircraft Design and Lightweight Structures
IPC	Institute of Polymers and Composites
FRP	Fibre-reinforced plastics
MPT	Multiaxial panel test machine
NDT	Non-destructive testing
RTM	Resin transfer moulding

References

1. Zimmermann, K.; Zenkert, D.; Siemetzki, M. Testing and analysis of ultra thick composites. *Compos. Part Eng.* **2010**, *41*, 326–336. [CrossRef]
2. de Vries, H. *Development of a Main Landing Gear Attachment Fitting Using Composite Material and RESIN transfer Moulding*; Technical Report; National Aerospace Laboratory NLR: Amsterdam, The Netherlands, 2009.
3. Luplow, T.; Protz, R.; Littner, L.; Drummer, J.; Kunze, E.; Heimbs, S.; Horst, P.; Gude, M.; Kreutzbruck, M.; Fiedler, B. Herausforderungen dickwandiger, duroplastischer Faser-Kunststoff-Verbunde in der Herstellung sowie mechanischen und zerstörungsfreien Prüfung-Ein Review. *Z. Kunststofftechnik* **2023**, *19*, 73–117. [CrossRef]
4. Martin, R.W.; Sabato, A.; Schoenberg, A.; Giles, R.H.; Niezrecki, C. Comparison of nondestructive testing techniques for the inspection of wind turbine blades' spar caps. *Wind. Energy* **2018**, *21*, 980–996. [CrossRef]
5. Lahuerta, F. Thickness Effect in Composite Laminates in Static and Fatigue Loading. Ph.D. Thesis, Universidad de Zaragoza, Zaragoza, Spain, 2016.
6. Lee, J.; Soutis, C. A study on the compressive strength of thick carbon fibre-epoxy laminates. *Compos. Sci. Technol.* **2007**, *67*, 2015–2026. [CrossRef]
7. Lahuerta, F.; Nijssen, R.P.; van der Meer, F.P.; Sluys, L.J. Thickness scaled compression tests in unidirectional glass fibre reinforced composites in static and fatigue loading. *Compos. Sci. Technol.* **2016**, *123*, 115–124. [CrossRef]
8. Yan, X. Finite element simulation of cure of thick composite: Formulations and validation verification. *J. Reinf. Plast. Compos.* **2008**, *27*, 339–355. [CrossRef]

9. Nsengiyumva, W.; Zhong, S.; Lin, J.; Zhang, Q.; Zhong, J.; Huang, Y. Advances, limitations and prospects of nondestructive testing and evaluation of thick composites and sandwich structures: A state-of-the-art review. *Compos. Struct.* **2021**, *256*, 112951. [CrossRef]
10. Maguire, J.M.; Sharp, N.D.; Pipes, R.B.; Brádaigh, C.M.Ó. Advanced process simulations for thick-section epoxy powder composite structures. *Compos. Part Appl. Sci. Manuf.* **2022**, *161*, 107073. [CrossRef]
11. Ekuase, O.A.; Anjum, N.; Eze, V.O.; Okoli, O.I. A review on the out-of-autoclave process for composite manufacturing. *J. Compos. Sci.* **2022**, *6*, 172. [CrossRef]
12. Komala, I.; van Campen, J.; Peeters, D.; Heimbs, S. Modeling the influence of fiber undulation in a filament-wound composite tube under radial crushing load. *Manuf. Lett.* **2025**, *43*, 51–54. [CrossRef]
13. Wisnom, M.R.; Atkinson, J.W. Reduction in tensile and flexural strength of unidirectional glass fibre-epoxy with increasing specimen size. *Compos. Struct.* **1997**, *38*, 405–411. [CrossRef]
14. Okabe, T.; Takeda, N. Size effect on tensile strength of unidirectional CFRP composites—Experiment and simulation. *Compos. Sci. Technol.* **2002**, *62*, 2053–2064. [CrossRef]
15. Bažant, Z.P.; Yu, Q. Universal size effect law and effect of crack depth on quasi-brittle structure strength. *J. Eng. Mech.* **2009**, *135*, 78–84. .) [CrossRef]
16. Camponeschi, E.T.; Gillespie, J.W.; Wilkins, D.J. Kink-band failure analysis of thick composites in compression. *J. Compos. Mater.* **1993**, *27*, 471–490. [CrossRef]
17. Soutis, C.; Curtis, P.T.; Fleck, N.A. Compressive failure of notched carbon fibre composites. *Proc. R. Soc. Lond. Ser. Math. Phys. Sci.* **1993**, *440*, 241–256. [CrossRef]
18. Soutis, C.; Lee, J.; Kong, C. Size effect on compressive strength of T300/924C carbon fibre-epoxy laminates. *Plast. Rubber Compos.* **2002**, *31*, 364–370. [CrossRef]
19. Bažant, Z.P.; Zhou, Y.; Novák, D.; Daniel, I.M. Size effect on flexural strength of fiber-composite laminates. *J. Eng. Mater. Technol.* **2004**, *126*, 29–37. [CrossRef]
20. Ganesan, R. Fatigue behavior of thick composite laminates. In *Fatigue Life Prediction of Composites and Composite Structures*; Elsevier: Amsterdam, The Netherlands, 2020; pp. 239–267. [CrossRef]
21. Hosoi, A.; Sakuma, S.; Seki, S.; Fujita, Y.; Taketa, I.; Kawada, H. Effect of stress ratio on fatigue characteristics in the out-of-plane direction of thick CFRP laminates with toughened interlaminar layers. In Proceedings of the 20th International Conference on Composite Materials, Copenhagen, Danemark, 19–24 July 2015.
22. Yan, G.; Lu, X.; Tang, J. Guided wave-based monitoring of evolution of fatigue damage in glass fiber/epoxy composites. *Appl. Sci.* **2019**, *9*, 1394. [CrossRef]
23. Solodov, I.; Bernhardt, Y.; Littner, L.; Kreutzbruck, M. Ultrasonic anisotropy in composites: Effects and applications. *J. Compos. Sci.* **2022**, *6*, 93. [CrossRef]
24. Fey, P.; Kreitzbruck, M. Quantification of fatigue state in CFRP using ultrasonic birefringence. *AIP Conf. Proc.* **2016**, *1706*, 050007. [CrossRef]
25. Kudryavtsev, O.; Guseinov, K.; Bezmelnitsyn, A.; Lomakin, E. Determination of interlaminar shear properties of fibre-reinforced composites under biaxial loading. *Polymers* **2022**, *14*, 2575. [CrossRef] [PubMed]
26. Broughton, W.R. *In-Plane Testing of Thick Composites: A Review*; Technical Report; National Physical Laboratory: Teddington, UK, 2006.
27. Found, M.S. A review of the multiaxial fatigue testing of fiber reinforced plastics. In *Multiaxial Fatigue: A Symposium*; ASTM International: Conshohocken, PA, USA, 1985; Volume STP853-EB, p. 381.
28. Vassilopoulos, A.P.; Keller, T. *Fatigue of Fiber-Reinforced Composites*; Springer Science & Business Media: Berlin/Heidelberg, Germany, 2011.
29. Tate, J.S.; Kelkar, A.D.; Whitcomb, J.D. Effect of braid angle on fatigue performance of biaxial braided composites. *Int. J. Fatigue* **2006**, *28*, 1239–1247. [CrossRef]
30. Montesano, J. Fatigue Damage Characterization of Braided and Woven Fiber Reinforced Polymer Matrix Composites at Room and Elevated Temperatures. Ph.D. Thesis, Ryerson University, Toronto, ON, Canada, 2012.
31. Swanson, S.R.; Smith, L.V. Comparison of the biaxial strength properties of braided and laminated carbon fiber composites. *Compos. Part Eng.* **1996**, *27*, 71–77. [CrossRef]
32. Drummer, J.; Luplow, T.; Littner, L.; Protz, R.; Heimbs, S.; Kreutzbruck, M.; Gude, M.; Fiedler, B. Influence of the position of fibre misalignment in glass fibre-reinforced polymers on mechanical properties, damage behaviour and traceability via non-destructive tests. *Composites Part C: Open Access* **2025**, *18*, 100633. [CrossRef]
33. Shahabaz, S.; Sharma, S.; Shetty, N.; Shetty, S.D.; MC, G. Influence of temperature on mechanical properties and machining of fibre reinforced polymer composites: A review. *Eng. Sci.* **2021**, *16*, 26–46. [CrossRef]
34. Reifsnider, K.L.; Stinchcomb, W.W. A critical-element model of the residual strength and life of fatigue-loaded composite coupons. In *Composite Materials: Fatigue and Fracture*; ASTM STP: Conshohocken, PA, USA, 1986; Volume 1012, pp. 3–23. [CrossRef]

35. Drummer, J.; Tafesh, F.; Fiedler, B. Effect of fiber misalignment and environmental temperature on the compressive behavior of fiber composites. *Polymers* **2023**, *15*, 2833. [CrossRef]
36. Protz, R.; Kosmann, N.; Fritsch, D.; Fey, P.; Essig, W.; Dietrich, K.; Gude, M.; Horst, P.; Kreutzbruck, M.; Schulte, K.; et al. Influence of voids and impact damage on the fatigue behaviour of large scale composites: Einfluss von Poren und Schlagschäden auf das Ermüdungsverhalten von Großstrukturen. *Mater. Werkst.* **2016**, *47*, 1058–1071. [CrossRef]
37. Littner, L.; Protz, R.; Kunze, E.; Bernhardt, Y.; Kreutzbruck, M.; Gude, M. Flow front monitoring in high-pressure resin transfer molding using phased array ultrasonic testing to optimize mold filling simulations. *Materials* **2024**, *17*, 207. [CrossRef] [PubMed]
38. *DIN EN ISO 14126:2024*; Fibre-Reinforced Plastic Composites—Determination of Compressive Properties in the In-Plane Direction. German Institute for Standardization (DIN): Beuth Verlag, Berlin, 2023.
39. Sutherland, H.J. *On the Fatigue Analysis of Wind Turbines*; Technical Report SAND99-0089; Sandia National Laboratories: Albuquerque, NM, USA; Livermore, CA, USA, 1999. [CrossRef]
40. Bangaru, A.K. Early Stage Fatigue Damage Mechanisms in Composite Material Used for Wind Turbine Rotor Blades. Ph.D. Thesis, DTU Wind Energy, Roskilde, Denmark, 2021. [CrossRef]